

Mechanism for unconventional superconductivity in the hole-doped Rashba-Hubbard model

Andrés Greco^{1,*} and Andreas P. Schnyder^{2,†}

¹Facultad de Ciencias Exactas, Ingeniería y Agrimensura and Instituto de Física Rosario (UNR-CONICET), Av. Pellegrini 250, 2000 Rosario, Argentina

²Max-Planck-Institute for Solid State Research, D-70569 Stuttgart, Germany

(Dated: May 1, 2018)

Motivated by the recent resurgence of interest in topological superconductivity, we study superconducting pairing instabilities of the hole-doped Rashba-Hubbard model on the square lattice with first- and second-neighbor hopping. Within the random phase approximation we compute the spin-fluctuation mediated paring interactions as a function of filling. Rashba spin-orbit coupling splits the spin degeneracies of the bands, which leads to two van Hove singularities at two different fillings. We find that for a doping region in between these two van Hove fillings the spin fluctuations exhibit a strong ferromagnetic contribution. Because of these ferromagnetic fluctuations, there is a strong tendency towards spin-triplet *f*-wave pairing within this filling region, resulting in a topologically nontrivial phase.

Topological superconductors (TSCs) have attracted great interest recently due to their potential use for quantum information technology and novel superconducting devices [1–6]. Many interesting topological phases, such as the chiral *p*-wave state [7], are realized in superconductors with odd-parity spin-triplet pairing. However, until now only a few material systems have been discovered which show spin-triplet superconductivity [8–10], since spin-singlet pairing is in most cases the dominant pairing channel. There are two types of TSCs with triplet pairing: intrinsic and artificial ones. While the former type arises as an intrinsic property of the material, the latter is artificially engineered in heterostructures by proximity coupling to an *s*-wave superconductor [11]. Intrinsic TSCs have the advantage that the topological phase exists in the entire volume of the material, and not just at an interface of a heterostructure. In recent years it has become clear that strong spin-orbit coupling (SOC) is conducive to triplet superconductivity [12–14]. Indeed, most candidate materials for intrinsic TSCs, such as Sr₂RuO₄ [8, 9], CePt₃Si [10], and Cu_xBi₂Se₃ [15, 16], contain heavy elements with strong spin-orbit interactions. Unfortunately, the strongly correlated TSCs Sr₂RuO₄ and CePt₃Si have a rather low *T_c* of $\lesssim 1$ K, while the pairing symmetry of the weakly correlated TSC Cu_xBi₂Se₃ is still under debate [17, 18]. Therefore, the search for new intrinsic TSCs remains an important goal.

Parallel to these developments, MBE fabrication of oxide and heavy-fermion superlattices has seen great progress [19–22]. An important distinguishing feature of epitaxial superlattices is their high tunability. That is, carrier density, Fermi surface (FS) topology, as well as SOC can be tuned by modulating the layer thickness or by applying electric fields [22, 23]. Remarkably, some of these superlattices show unconventional superconductivity with a fairly high-transition temperature. One example is the heavy-fermion superlattice

CeCoIn₅/YbCoIn₅ [21, 22], in which magnetic fluctuations [24] lead to superconductivity below $T_c \simeq 2$ K. Modulating the layer thicknesses in this superlattice breaks the inversion symmetry, which induces Rashba spin-orbit interactions. Interestingly, the strength of the Rashba SOC can be controlled by the width of the YbCoIn₅ block layers. Strong Rashba interaction drastically alters the FS topology by splitting the spin degeneracy. This in turn is favorable for triplet superconductivity, provided that the pairing mechanism allows for it. As is known from extensive theoretical works on cuprate superconductors [25–27], the shape and topology of the FS strongly influence the relative strengths of different pairing channels. In order to optimize the layer thickness modulation in CeCoIn₅/YbCoIn₅ for triplet superconductivity, it is therefore important to understand the detailed interdependence among Rashba SOC, FS topology, and superconducting pairing symmetry.

Motivated by these considerations, we analyze in this Letter superconducting pairing instabilities of the hole-doped Rashba-Hubbard model, which describes the essential features of many strongly correlated materials with Rashba SOC [12–14, 28]. Focusing on the square lattice with first- and second-neighbor hopping, *t* and *t'*, we compute the spin-fluctuation-mediated pairing interaction as a function of filling. For this purpose we use the random phase approximation (RPA), which is known to qualitatively capture the essential physics, at least within weak coupling [12–14, 25–27]. Finite SOC splits the energy bands leading to two van Hove singularities at the fillings n_{vH_1} and n_{vH_2} . Remarkably, we find that in a doping region in between these two van Hove fillings, there exist strong *ferromagnetic* (FM) spin fluctuations (Figs. 1 and 2). Due to these FM fluctuations there is a strong tendency towards spin-triplet *f*-wave pairing in this filling region, while the pairing channels of *d*-wave type (Fig. 3) are of the same order or subdominant.

Model and Method.— The Rashba-Hubbard model on

the square lattice is given

$$H = \sum_{\mathbf{k}} \psi_{\mathbf{k}}^\dagger \hat{h}(\mathbf{k}) \psi_{\mathbf{k}} + U \sum_{\mathbf{k}, \mathbf{k}', \mathbf{q}} c_{\mathbf{k}\uparrow}^\dagger c_{\mathbf{k}+\mathbf{q}\uparrow} c_{\mathbf{k}'\downarrow}^\dagger c_{\mathbf{k}'-\mathbf{q}\downarrow}, \quad (1)$$

where U is the local Coulomb repulsion, $\hat{h}(\mathbf{k}) = (\varepsilon_{\mathbf{k}}\tau_0 + \mathbf{g}_{\mathbf{k}} \cdot \boldsymbol{\tau})$, and $\psi_{\mathbf{k}} = (c_{\mathbf{k}\uparrow}, c_{\mathbf{k}\downarrow})^T$. Here, $\boldsymbol{\tau} = (\tau_1, \tau_2, \tau_3)^T$ are the three Pauli matrices, and τ_0 stands for the 2×2 unit matrix. The band energy $\varepsilon_{\mathbf{k}} = -2t(\cos k_x + \cos k_y) + t' \cos k_x \cos k_y - \mu$ contains both first- and second-neighbor hopping, t and t' , respectively, and is measured relative to the chemical potential μ . The vector $\mathbf{g}_{\mathbf{k}}$ describes Rashba SOC with $\mathbf{g}_{\mathbf{k}} = V_{\text{so}}(\partial\varepsilon_{\mathbf{k}}/\partial k_y, -\partial\varepsilon_{\mathbf{k}}/\partial k_x, 0)$ and the coupling constant V_{so} . For our numerical calculations we set $t = 1$, $t' = 0.3$, and $V_{\text{so}} = 0.5$, and focus on the hole-doped case with filling $0.4 < n < 1$. We have checked that other parameter choices do no qualitatively change our findings. The presence of Rashba SOC splits the electronic dispersion $\varepsilon_{\mathbf{k}}$ into negative- and positive-helicity bands with energies $E_{\mathbf{k}}^1 = \varepsilon_{\mathbf{k}} - |\mathbf{g}_{\mathbf{k}}|$ and $E_{\mathbf{k}}^2 = \varepsilon_{\mathbf{k}} + |\mathbf{g}_{\mathbf{k}}|$, respectively. Both spin-split bands exhibit van Hove singularities at $\mathbf{k} = (\pi, 0)$ and symmetry related points. For our parameter choice the corresponding van Hove fillings occur at $n_{vH_1} \simeq 0.87$ and $n_{vH_2} \simeq 0.65$, see inset of Fig. 2.

The first term of Eq. 1 defines the bare 2×2 fermionic Greens function in the spin basis

$$G_{\sigma_1\sigma_2}^{(0)}(\mathbf{k}, i\nu_n) = \left(\left[i\nu_n \tau_0 - \hat{h}(\mathbf{k}) \right]^{-1} \right)_{\sigma_1\sigma_2}, \quad (2)$$

where $\nu_n = 2n\pi/\beta$ is the fermionic Matsubara frequency. For $U = 0$ the bare spin susceptibility can be expressed in terms of $G^{(0)}$ as

$$\chi_{\sigma_1\sigma_2\sigma_3\sigma_4}^{(0)}(\mathbf{q}, i\omega_l) = \sum_{\mathbf{k}, i\nu_n} G_{\sigma_1\sigma_2}^{(0)}(\mathbf{k}, i\nu_n) G_{\sigma_3\sigma_4}^{(0)}(\mathbf{k}+\mathbf{q}, i\nu_n + i\omega_l), \quad (3)$$

where $\omega_l = 2l\pi/\beta$ is the bosonic Matsubara frequency. Within the RPA [12, 13] the dressed spin susceptibility $\chi_{\sigma_1\sigma_2\sigma_3\sigma_4}(\mathbf{q}, i\omega_l)$ is computed as

$$\hat{\chi}(\mathbf{q}, i\omega_l) = \left[\mathbb{1} - \hat{\chi}^{(0)}(\mathbf{q}, i\omega_l) \hat{U} \right]^{-1} \hat{\chi}^{(0)}(\mathbf{q}, i\omega_l). \quad (4)$$

In Eq. (4) the sixteen components of $\chi_{\sigma_1\sigma_2\sigma_3\sigma_4}$ and $\chi_{\sigma_1\sigma_2\sigma_3\sigma_4}^{(0)}$ are stored in the 4×4 matrices $\hat{\chi}$ and $\chi^{(0)}$, respectively, and the 4×4 coupling matrix \hat{U} is antidiagonal, see the Supplemental Material (SM) [29] for details.

The spin fluctuations described by Eq. (4) can lead to an effective interaction that combines two electrons into a Cooper pair. As in Refs. 25, 26, it is necessary to distinguish between the interaction for same [$V_{\text{same}}^{\text{eff}}(\mathbf{k}, \mathbf{k}')$] and for opposite [$V_{\text{opp}}^{\text{eff}}(\mathbf{k}, \mathbf{k}')$] spin projections between two electrons with momentum \mathbf{k} and \mathbf{k}' [30], which are given in the spin basis by

$$V_{\text{same}}^{\text{eff}}(\mathbf{k}, \mathbf{k}') = U^2 \chi_{\sigma\sigma\sigma\sigma}(\mathbf{k} - \mathbf{k}'), \quad (5a)$$

$$V_{\text{opp}}^{\text{eff}}(\mathbf{k}, \mathbf{k}') = U^2 \chi_{\sigma\bar{\sigma}\bar{\sigma}\sigma}(\mathbf{k} - \mathbf{k}') + U^2 \chi_{\sigma\sigma\bar{\sigma}\bar{\sigma}}(\mathbf{k} + \mathbf{k}') \quad (5b)$$

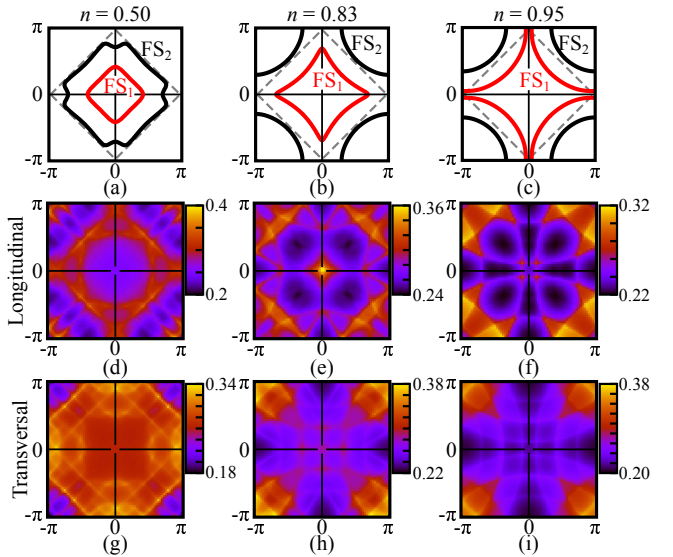


FIG. 1: (a)-(c) Calculated Fermi surface topology and (d)-(i) static $\omega = 0$ spin susceptibility for the fillings $n = 0.50$, $n = 0.83$, and $n = 0.95$, with $t' = 0.3$, $V_{\text{so}} = 0.5$, $T = 0.01$, and $U = 0.4$. The second and third rows show the longitudinal and transversal susceptibilities, $\chi_{\text{long}} = \chi_{\uparrow\uparrow\uparrow\uparrow} - \chi_{\uparrow\downarrow\downarrow\uparrow}$ and $\chi_{\text{trans}} = \chi_{\uparrow\uparrow\downarrow\downarrow}$, respectively (see SM [29]).

respectively. In weak coupling we can define for each pairing channel i a dimensionless pairing strength as [31–34]

$$\lambda_i^{\alpha\beta} = - \frac{\int_{\text{FS}_\alpha} \frac{dk}{v_F^\alpha(k)} \int_{\text{FS}_\beta} \frac{dk'}{v_F^\beta(k')} \eta_i(k) V_{s/t}^{\text{eff}}(k, k') \eta_i(k')}{2\pi^2 \int_{\text{FS}_\beta} \frac{dk'}{v_F^\beta(k')} [\eta_i(k')]^2}, \quad (6)$$

where α and β label the FS sheets. The diagonal and off-diagonal elements of $\lambda_i^{\alpha\beta}$ represent intra- and inter Fermi surface pairing strengths, respectively. In Eq. (6), k and k' are restricted to the Fermi sheets FS_α and FS_β , respectively, $v_F^\alpha(\mathbf{k}) = |\nabla_{\mathbf{k}} E_\mathbf{k}^\alpha|$ is the Fermi velocity, and $\eta_i(k)$ describes the k dependence of each possible pairing symmetry, see SM [29]. In the case of singlet pairing the effective interaction in Eq. (6) is solely due to scattering between electrons with opposite spins. For triplet pairing, however, both same- and opposite-spin scattering processes are possible. The effective superconducting coupling constant λ_i^{eff} for a given pairing channel i is given by the largest eigenvalue of the matrix $\lambda_i^{\alpha\beta}$ [32]. Hence, by numerically evaluating Eq. (6) for all possible channels i we can identify the leading pairing instability as a function of filling and SOC strength.

Spin susceptibility.— Before discussing superconductivity, let us first consider the static susceptibility in the paramagnetic state for intermediate coupling $U = 0.4$ and $T = 0.01$. While Figs. 1(d)-1(f) show the longitudinal susceptibility, Figs. 1(g)-1(i) show the transversal susceptibility for the fillings $n = 0.5$, $n = 0.83$, and

$n = 0.95$, respectively. As expected, and different to the case without SOC, the longitudinal and transversal susceptibilities show different spin texture. The FS topology for each filling is shown in Figs. 1(a)-1(c). The spin susceptibility shows large magnetic fluctuations, whose magnetic modulation vectors \mathbf{q} depend strongly on filling n and FS topology. Indeed, we observe an intricate interplay between FS topology and the structure of the spin susceptibility: For $n > n_{vH_1}$ the two spin-split FS sheets are hole-like and centered at (π, π) [Fig. 1(c)], which results in a spin susceptibility with incommensurate anti-ferromagnetic modulation vector $\mathbf{q} = (\pi, \pi \pm \delta)$, see Figs. 1(f), and 1(i). For $n < n_{vH_2}$, on the other hand, both FS sheets are electron-like and centered at Γ [Fig. 1(a)] leading to a longitudinal spin susceptibility with nearly commensurate anti-ferromagnetic \mathbf{q} vector [Fig. 1(d)]. In between the two van Hove fillings, $n_{vH_2} < n < n_{vH_1}$, FS₁ is electron-like and centered at Γ , while FS₂ is hole-like and centered at (π, π) , see Fig. 1(b). Interestingly, within this filling range there exists a broad region, i.e., $0.76 \lesssim n \lesssim n_{vH_1}$, where the dominant longitudinal fluctuations are ferromagnetic with $\mathbf{q} = (0, 0)$, see Figs. 1(e) and 2.

Increasing the Hubbard interaction U enhances the magnetic fluctuations and eventually drives the system into the magnetically ordered phase. In this process the modulation vector of the strongest fluctuations becomes the ordering wave vector of the ordered phase. The transition between paramagnetic and ordered phase occurs at the critical interaction strength U_c with a given ordering wave vector where the susceptibility diverges. Although the transversal and longitudinal susceptibilities show different spin texture, both diverge simultaneously at the same ordering momentum, showing the non trivial feedback between them for finite SOC. Figure 2 displays the filling dependence of the critical interaction U_c (red line). The color scale indicates the intensity of the ferromagnetic fluctuations in the longitudinal susceptibility relative to the (incommensurate) antiferromagnetic fluctuations. We observe that the ferromagnetic fluctuations are dominant in the filling range $0.76 \lesssim n \lesssim n_{vH_1}$ and for U within the range $0 \leq U \lesssim 1.6$. These ferromagnetic fluctuations originate from the combined effect of finite SOC V_{so} and finite t' . As a matter of fact, for $V_{\text{so}} = 0$ and $t' \neq 0$ there is only one van Hove filling at $n_{vH} \sim 0.72$ (inset of Fig. 2), which separates commensurate antiferromagnetism [$\mathbf{q} = (\pi, \pi)$] for $n > n_{vH}$ from incommensurate antiferromagnetism [$\mathbf{q} = (\pi, \pi - \delta)$] for $n < n_{vH}$, and ferromagnetic fluctuations only occur in a narrow region around the van Hove filling n_{vH} [25]. For $t' = 0$ and $V_{\text{so}} \neq 0$ ferromagnetic fluctuations are absent [14]. Different to the longitudinal susceptibility the transversal susceptibility shows ferromagnetic fluctuations only very close to the van Hove fillings n_{vH_1} and n_{vH_2} [Fig. S5 of the SM].

Superconducting instabilities.— The discussed mag-

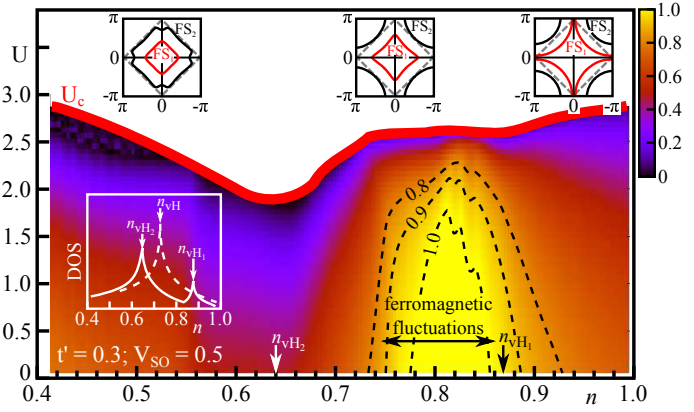


FIG. 2: The critical interaction strength U_c as a function of filling n is indicated by the red line. The color scale represents the relative intensity of the ferromagnetic fluctuations in the longitudinal susceptibility. The inset shows the density of states versus filling for $V_{\text{so}} = 0$ (dashed line) and $V_{\text{so}} = 0.5$ (solid line).

netic fluctuations can lead to superconducting pairing instabilities. We set the Hubbard interaction to $U = 0.4 < U_c$ and compute λ_i^{eff} within the filling range $0.4 < n < 1$ for the lowest-harmonic pairing symmetries, as defined in Eq. (S11) of the SM. The resulting filling dependence of the pairing symmetries is presented in Fig. 3. Note that the weak coupling approach is more reliable away from the van Hove fillings. At the van Hove fillings n_{vH_i} , λ_i^{eff} exhibits large jumps due to the divergent density of states [35], which is an artifact of the weak coupling approach. Let us examine the results of Fig. 3 separately for (i) $n > n_{vH_1}$, (ii) $n < n_{vH_2}$, and (iii) $n_{vH_2} < n < n_{vH_1}$:

(i) $n > n_{vH_1}$: For this filling region the singlet $d_{x^2-y^2}$ -wave pairing channel is dominant. This is due to large anti-ferromagnetic spin fluctuations that exist in the entire hole-doping range $1 > n > n_{vH_1}$, similar to the case of $V_{\text{so}} = 0$ [25]. The subleading pairing solutions have p -wave and f -wave symmetry due to effective interactions with same spin projections. Notice that in contrast to the case for $V_{\text{so}} = 0$ [25], here the pairing strength for same spin projections is different from opposite spin projections. While the tendency to superconductivity in the f -wave channel is strongly decreasing approaching half-filling, it is rather stable for the p -wave channel. Because Rashba SOC breaks inversion symmetry, we expect that in this filling range the pairing symmetry is an admixture of $d_{x^2-y^2}$ -wave, p -wave, and f -wave [36]. However, since $\lambda_{d_{x^2-y^2}}^{\text{eff}} \gg \lambda_{p/f}^{\text{eff}}$, the $d_{x^2-y^2}$ -wave channel is the leading one.

(ii) $n < n_{vH_2}$: In this filling region the d_{xy} -wave pairing is leading, while the f -wave and p -wave channels are subdominant. We ascribe this tendency towards d_{xy} -wave pairing, rather than $d_{x^2-y^2}$ -wave, to the strong transversal spin fluctuations, which are peaked at $(\pi, 0)$ and symmetry related points.

(iii) $n_{vH_2} < n < n_{vH_1}$: This is the most interesting region. Remarkably, we find that around the filling $n \simeq 0.78$ the triplet f -wave solution for same spin projections is the leading one, which we attribute to the strong ferromagnetic fluctuations that occur for this filling in the longitudinal susceptibility [cf. Figs. 1(e) and 2]. The subdominant pairing channels have $d_{x^2-y^2}$ -wave and d_{xy} -wave form. Hence, due to broken inversion symmetry, the gap is expected to exhibit also d -wave admixture to the dominant f -wave harmonic. Although the weak coupling RPA approach underestimates the values of λ_i^{eff} , it nevertheless qualitatively captures the relative tendency to superconductivity in each channel. Different to the case for $V_{\text{so}} = 0$ [25], where ferromagnetic fluctuations occur only very close to the van Hove filling and a singular behavior is found at this filling for triplet f -wave pairing, here triplet f -wave extends in a broad filling region. This fact rules out the possibility that the observed tendency towards f -wave pairing is an artifact of the van Hove singularity. Without second-neighbor hopping the triplet pairing component is always subdominant [14]. Thus, our results offer a microscopic mechanism for the realization of triplet pairing with same spin projection, which was proposed on phenomenological grounds to be a candidate in non-centrosymmetric systems with strong SOC [36].

To analyze the dominance of the triplet f -wave channel we show in Fig. 3(b) the dependence of λ_i^{eff} on the interaction strength U for $n = 0.78$. We find that λ_f^{eff} is the largest effective coupling for $0.0 < U \lesssim 0.5$. This behavior is consistent with the result of Fig. 2 which shows that the ferromagnetic fluctuations become less and less dominant with increasing U . Before concluding, let us briefly discuss the contributions of the intra and inter FS scattering processes to the effective superconducting coupling. In Figs. 3(c) we present the filling dependence of the intra FS (λ_i^{11} and λ_i^{22}) and the inter FS (λ_i^{12}) pairing strengths for the f -wave channel for same spin projections [29]. We observe that the f -wave pairing is driven by intra FS processes within FS₂.

Conclusions and implications for experiments.— We have studied superconducting instabilities of the hole-doped Rashba-Hubbard model with first- and second-neighbor hopping within a spin-fluctuation-mediated pairing scenario. Using an RPA approach, we have determined the pairing symmetry as a function of filling and have shown that there exists an interplay between FS topology, structure of the magnetic fluctuations, and pairing symmetry. In between the two van Hove fillings, close to $n \simeq 0.78$, the leading pairing solution has triplet f -wave symmetry, which is driven by ferromagnetic fluctuations. Since within the spin fluctuation scenario the pairing symmetry is largely determined by the type of spin fluctuations, we expect that more sophisticated treatments, such as FLEX [37] or fRG [38], will confirm our RPA analysis. The tendency towards f -wave

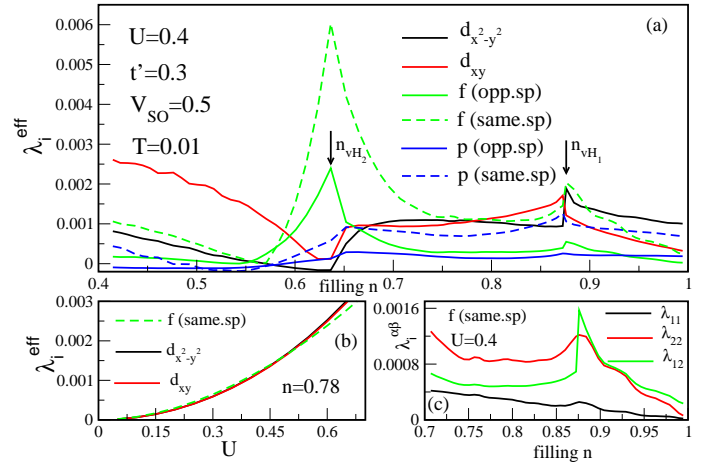


FIG. 3: (a) Filling dependence of the superconducting couplings λ_i^{eff} , as determined from Eq. (6) for $U = 0.4$, and for the lowest-harmonic pairing symmetries given by Eq. (S11). Here, we do not show the s -wave pairing channel, since it is highly suppressed (i.e., negative) for the entire hole-doping range. For the numerical evaluation of Eq. (6) we used 408 Fermi momenta. (b) λ_i^{eff} versus U for the filling $n = 0.78$. We present results up to $U = 0.7$ to show the regime where f -wave is dominant. With increasing U the curves increase monotonically, and d -wave becomes dominant while f -wave subdominant for $U \gtrsim 0.5$. Near the magnetic instability $U = U_c$ we find that $\lambda_d^{\text{eff}} \sim 0.2$ and $\lambda_f^{\text{eff}} \sim 0.15$. (c) Filling dependence of the intra and inter FS pairing strengths, $\lambda_i^{\alpha\alpha}$ and $\lambda_i^{\alpha\beta}$, for the f -wave channel with same spin projections.

pairing near $n \simeq 0.78$ unavoidably leads to a topologically nontrivial state. The precise nature of this topological state depends on the detailed momentum structure of the gap. There are three possibilities: (i) The superconducting state is nodal with a dominant f -wave pairing symmetry and only small admixtures of d -wave and p -wave components. The point nodes of this superconducting state are topologically protected by a winding number, which gives rise to Majorana flat band edge states [5]. (ii) The superconducting state is fully gapped due to a sizable admixture of d -wave and p -wave components. In this case the superconducting state belongs to symmetry class DIII and exhibits helical Majorana edge states [1]. (iii) The non-linear gap equation has a complex solution, yielding a time-reversal breaking triplet pairing state without nodes. This corresponds to a topological superconductor in symmetry class D, with chiral Majorana edge states [1]. In closing we note that pair decoherence caused by impurity scattering is suppressed in all of the above three scenarios, due to the spin-momentum locking of the band structure [39].

Our findings provide a new mechanism for the creation of triplet superconductivity, which is relevant for non-centrosymmetric superconductors with strong SOC [5, 10] and for oxide and heavy-fermion hybrid structures [19–22]. It might be possible to realize the dis-

cussed *f*-wave state in CeCoIn₅/YbCoIn₅ hybrid structures [21, 22], by an appropriate choice of layer thickness modulation. We hope that the present study will stimulate further experimental investigations along these directions.

Acknowledgments.— We thank M. Bejas, H. Nakamura, J. Riera, A. T. Rømer, T. Yokoyama, and R. Zeyher for useful discussions. A.G. thanks the Max Planck Institute for Solid State Research in Stuttgart for hospitality and financial support.

* agreco@fceia.unr.edu.ar
 † a.schnyder@flkf.mpg.de

[1] C.-K. Chiu, J. C. Y. Teo, A. P. Schnyder, and S. Ryu, Rev. Mod. Phys. **88**, 035005 (2016), URL <https://link.aps.org/doi/10.1103/RevModPhys.88.035005>.

[2] M. Z. Hasan and C. L. Kane, Rev. Mod. Phys. **82**, 3045 (2010).

[3] X.-L. Qi and S.-C. Zhang, Rev. Mod. Phys. **83**, 1057 (2011).

[4] A. P. Schnyder, S. Ryu, A. Furusaki, and A. W. W. Ludwig, Phys. Rev. B **78**, 195125 (2008).

[5] A. P. Schnyder and P. M. R. Brydon, Journal of Physics: Condensed Matter **27**, 243201 (2015), URL <http://stacks.iop.org/0953-8984/27/i=24/a=243201>.

[6] M. Sato and Y. Ando, ArXiv e-prints (2016), 1608.03395.

[7] N. Read and D. Green, Phys. Rev. B **61**, 10267 (2000), URL <https://link.aps.org/doi/10.1103/PhysRevB.61.10267>.

[8] C. Kallin and J. Berlinsky, Reports on Progress in Physics **79**, 054502 (2016), URL <http://stacks.iop.org/0034-4885/79/i=5/a=054502>.

[9] Y. Maeno, S. Kittaka, T. Nomura, S. Yonezawa, and K. Ishida, Journal of the Physical Society of Japan **81**, 011009 (2012), <http://dx.doi.org/10.1143/JPSJ.81.011009>, URL <http://dx.doi.org/10.1143/JPSJ.81.011009>.

[10] M. Smidman, M. B. Salamon, H. Q. Yuan, and D. F. Agterberg, Reports on Progress in Physics **80**, 036501 (2017), URL <http://stacks.iop.org/0034-4885/80/i=3/a=036501>.

[11] L. Fu and C. L. Kane, Phys. Rev. Lett. **100**, 096407 (2008), URL <https://link.aps.org/doi/10.1103/PhysRevLett.100.096407>.

[12] Y. Yanase and M. Sigrist, Journal of the Physical Society of Japan **76**, 043712 (2007), URL <http://dx.doi.org/10.1143/JPSJ.76.043712>.

[13] Y. Yanase and M. Sigrist, Journal of the Physical Society of Japan **77**, 124711 (2008), <http://dx.doi.org/10.1143/JPSJ.77.124711>, URL <http://dx.doi.org/10.1143/JPSJ.77.124711>.

[14] T. Yokoyama, S. Onari, and Y. Tanaka, Phys. Rev. B **75**, 172511 (2007), URL <https://link.aps.org/doi/10.1103/PhysRevB.75.172511>.

[15] Y. S. Hor, A. J. Williams, J. G. Checkelsky, P. Roushan, J. Seo, Q. Xu, H. W. Zandbergen, A. Yazdani, N. P. Ong, and R. J. Cava, Phys. Rev. Lett. **104**, 057001 (2010), URL <https://link.aps.org/doi/10.1103/PhysRevLett.104.057001>.

[16] S. Sasaki, M. Kriener, K. Segawa, K. Yada, Y. Tanaka, M. Sato, and Y. Ando, Phys. Rev. Lett. **107**, 217001 (2011), URL <https://link.aps.org/doi/10.1103/PhysRevLett.107.217001>.

[17] N. Levy, T. Zhang, J. Ha, F. Sharifi, A. A. Talin, Y. Kuk, and J. A. Stroscio, Phys. Rev. Lett. **110**, 117001 (2013), URL <https://link.aps.org/doi/10.1103/PhysRevLett.110.117001>.

[18] P. M. R. Brydon, S. Das Sarma, H.-Y. Hui, and J. D. Sau, Phys. Rev. B **90**, 184512 (2014), URL <https://link.aps.org/doi/10.1103/PhysRevB.90.184512>.

[19] J. Chakhalian, J. W. Freeland, H.-U. Habermeier, G. Cristiani, G. Khalilullin, M. van Veenendaal, and B. Keimer, Science **318**, 1114 (2007), ISSN 0036-8075, <http://science.sciencemag.org/content/318/5853/1114.full.pdf>, URL <http://science.sciencemag.org/content/318/5853/1114>.

[20] N. Reyren, S. Thiel, A. D. Caviglia, L. F. Kourkoutis, G. Hammerl, C. Richter, C. W. Schneider, T. Kopp, A.-S. Rüetschi, D. Jaccard, et al., Science **317**, 1196 (2007), ISSN 0036-8075, <http://science.sciencemag.org/content/317/5842/1196.full.pdf>, URL <http://science.sciencemag.org/content/317/5842/1196>.

[21] Y. Mizukami, H. Shishido, T. Shibauchi, M. Shimozawa, S. Yasumoto, D. Watanabe, M. Yamashita, H. Ikeda, T. Terashima, H. Kontani, et al., Nat Phys **7**, 849 (2011), URL <http://dx.doi.org/10.1038/nphys2112>.

[22] M. Shimozawa, S. K. Goh, R. Endo, R. Kobayashi, T. Watashige, Y. Mizukami, H. Ikeda, H. Shishido, Y. Yanase, T. Terashima, et al., Phys. Rev. Lett. **112**, 156404 (2014), URL <https://link.aps.org/doi/10.1103/PhysRevLett.112.156404>.

[23] A. D. Caviglia, S. Gariglio, N. Reyren, D. Jaccard, T. Schneider, M. Gabay, S. Thiel, G. Hammerl, J. Mannhart, and J. M. Triscone, Nature **456**, 624 (2008), URL <http://dx.doi.org/10.1038/nature07576>.

[24] C. Stock, C. Broholm, J. Hudis, H. J. Kang, and C. Petrovic, Phys. Rev. Lett. **100**, 087001 (2008), URL <https://link.aps.org/doi/10.1103/PhysRevLett.100.087001>.

[25] A. T. Rømer, A. Kreisel, I. Eremin, M. A. Malakhov, T. A. Maier, P. J. Hirschfeld, and B. M. Andersen, Phys. Rev. B **92**, 104505 (2015), URL <https://link.aps.org/doi/10.1103/PhysRevB.92.104505>.

[26] D. J. Scalapino, E. Loh, and J. E. Hirsch, Phys. Rev. B **34**, 8190 (1986), URL <https://link.aps.org/doi/10.1103/PhysRevB.34.8190>.

[27] R. Hlubina, Phys. Rev. B **59**, 9600 (1999), URL <https://link.aps.org/doi/10.1103/PhysRevB.59.9600>.

[28] G. A. Meza and J. A. Riera, Phys. Rev. B **90**, 085107 (2014), URL <https://link.aps.org/doi/10.1103/PhysRevB.90.085107>.

[29] See Supplemental Material for a derivation of Eqs. (4), (5), and (6) and additional plots of the spin susceptibility and the pairing strengths.

[30] Since we focus on weak coupling, it is sufficient to consider only the static $\omega = 0$ pairing interaction.

[31] P. A. Frigeri, D. F. Agterberg, I. Milat, and M. Sigrist, The European Physical Journal B - Condensed Matter and Complex Systems **54**, 435 (2006), ISSN 1434-6036, URL <http://dx.doi.org/10.1140/epjb/e2007-00019-5>.

[32] O. V. Dolgov and A. A. Golubov, Phys. Rev. B **77**, 214526 (2008), URL <https://link.aps.org/doi/10.1103/PhysRevB.77.214526>.

- [33] O. V. Dolgov, I. I. Mazin, D. Parker, and A. A. Golubov, Phys. Rev. B **79**, 060502 (2009), URL <https://link.aps.org/doi/10.1103/PhysRevB.79.060502>.
- [34] P. J. Hirschfeld, M. M. Korshunov, and I. I. Mazin, Reports on Progress in Physics **74**, 124508 (2011), URL <http://stacks.iop.org/0034-4885/74/i=12/a=124508>.
- [35] The weak coupling approach neglects retardations and restricts the momenta to the Fermi surfaces. This makes the calculation of λ_i , Eq. (6), overly sensitive to the density of states, which is large very close to the van Hove fillings. For this reason the weak coupling approach should be considered with care close to n_{vH_i} .
- [36] P. A. Frigeri, D. F. Agterberg, A. Koga, and M. Sigrist, Phys. Rev. Lett. **92**, 097001 (2004), URL <https://link.aps.org/doi/10.1103/PhysRevLett.92.097001>.
- [37] Y. Yanase, T. Jujo, T. Nomura, H. Ikeda, T. Hotta, and K. Yamada, Physics Reports **387**, 1 (2003), ISSN 0370-1573, URL <http://www.sciencedirect.com/science/article/pii/S0370157303003235>.
- [38] W. Metzner, M. Salmhofer, C. Honerkamp, V. Meden, and K. Schönhammer, Rev. Mod. Phys. **84**, 299 (2012), URL <https://link.aps.org/doi/10.1103/RevModPhys.84.299>.
- [39] In Ref. [40] it was shown that spin-orbit locking protects three-dimensional odd-parity superconductors against disorder, due to an emergent chiral symmetry. A similar protection mechanism is expected to occur in the Rashba-Hubbard model. A detailed study of this is left for further investigations.
- [40] K. Michaeli and L. Fu, Phys. Rev. Lett. **109**, 187003 (2012), URL <https://link.aps.org/doi/10.1103/PhysRevLett.109.187003>.

**Supplemental material:
Mechanism for unconventional superconductivity in the hole-doped Rashba-Hubbard model**

Andrés Greco¹ and Andreas P. Schnyder²

¹*Facultad de Ciencias Exactas, Ingeniería y Agrimensura and Instituto de Física Rosario (UNR-CONICET), Av. Pellegrini 250, 2000 Rosario, Argentina*

²*Max-Planck-Institute for Solid State Research, D-70569 Stuttgart, Germany*

In this supplemental material we give details of the derivation of the RPA spin susceptibility and the effective pairing interactions. We also present additional plots of the spin susceptibility and the pairing strengths λ_i^{eff} .

I. DERIVATION OF THE RPA SPIN SUSCEPTIBILITY

Within the RPA the spin susceptibility $\chi_{\sigma_1\sigma_2\sigma_3\sigma_4}(\mathbf{q}, i\omega_l)$ in the spin basis is obtained from an infinite sum of bubble and ladder diagrams, as shown in Fig. S1. The solid lines in the diagrams correspond to the bare 2×2 fermion propagator $G_{\sigma_1\sigma_2}^{(0)}(\mathbf{k}, i\nu_n)$ [see Eq. (S2) and Fig. S2(a)] and the dashed lines are the bare vertex U [see Fig. S2 (b)]. The bare susceptibility, represented by a single bubble in Fig. S1, is given by

$$\chi_{\sigma_1\sigma_2\sigma_3\sigma_4}^{(0)}(\mathbf{q}, i\omega_l) = \sum_{\mathbf{k}, i\nu_n} G_{\sigma_1\sigma_2}^{(0)}(\mathbf{k}, i\nu_n) G_{\sigma_3\sigma_4}^{(0)}(\mathbf{k} + \mathbf{q}, i\nu_n + i\omega_l), \quad (\text{S1})$$

with ω_l the bosonic Matsubara frequency, and

$$G_{\sigma_1\sigma_2}^{(0)}(\mathbf{k}, i\nu_n) = \left(\left[i\nu_n \sigma_0 - \hat{h}(\mathbf{k}) \right]^{-1} \right)_{\sigma_1\sigma_2} \quad (\text{S2})$$

the 2×2 bare Greens function with $\nu_n = (2n+1)\pi/\beta$ the fermionic Matsubara frequency. Arranging the sixteen

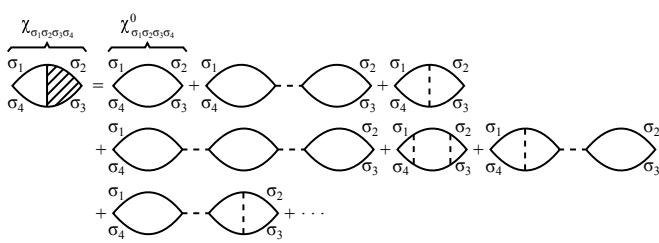


FIG. S1: The spin susceptibility $\chi_{\sigma_1\sigma_2\sigma_3\sigma_4}$ is calculated within RPA as a sum of bubbles and ladders. In the diagrams only external indices ($\sigma_1, \sigma_2, \sigma_3$, and σ_4) are indicated. Internal indices or omitted and are assumed to be summed over. Note that due to finite SOC the contributions from bubble and ladder diagrams are mixed, which is in contrast to the case without SOC [25, 26].

matrix elements of $\chi_{\sigma_1\sigma_2\sigma_3\sigma_4}^{(0)}$ in a 4×4 matrix,

$$\hat{\chi}^{(0)} = \begin{pmatrix} \chi_{\uparrow\uparrow\uparrow\uparrow}^{(0)} & \chi_{\uparrow\uparrow\uparrow\uparrow}^{(0)} & \chi_{\uparrow\uparrow\uparrow\uparrow}^{(0)} & \chi_{\uparrow\uparrow\uparrow\uparrow}^{(0)} \\ \chi_{\uparrow\uparrow\uparrow\downarrow}^{(0)} & \chi_{\uparrow\uparrow\downarrow\downarrow}^{(0)} & \chi_{\uparrow\uparrow\downarrow\downarrow}^{(0)} & \chi_{\uparrow\downarrow\downarrow\downarrow}^{(0)} \\ \chi_{\downarrow\uparrow\uparrow\uparrow}^{(0)} & \chi_{\downarrow\uparrow\uparrow\uparrow}^{(0)} & \chi_{\downarrow\uparrow\uparrow\uparrow}^{(0)} & \chi_{\downarrow\uparrow\uparrow\uparrow}^{(0)} \\ \chi_{\downarrow\uparrow\uparrow\downarrow}^{(0)} & \chi_{\downarrow\uparrow\downarrow\downarrow}^{(0)} & \chi_{\downarrow\uparrow\downarrow\downarrow}^{(0)} & \chi_{\downarrow\downarrow\downarrow\downarrow}^{(0)} \end{pmatrix}, \quad (\text{S3})$$

the infinite sum in Fig. S1 can be expressed analytically as [13]

$$\hat{\chi}(\mathbf{q}, i\omega_l) = \left[I - \hat{\chi}^{(0)}(\mathbf{q}, i\omega_l) \hat{U} \right]^{-1} \hat{\chi}^{(0)}(\mathbf{q}, i\omega_l), \quad (\text{S4})$$

where the dressed 4×4 matrix $\hat{\chi}$ contains the sixteen dressed susceptibilities arranged in similar form as in $\hat{\chi}^{(0)}$. The 4×4 interaction matrix \hat{U} in Eq. (S4) is off-diagonal with

$$\hat{U} = \begin{pmatrix} 0 & 0 & 0 & U \\ 0 & 0 & -U & 0 \\ 0 & -U & 0 & 0 \\ U & 0 & 0 & 0 \end{pmatrix}. \quad (\text{S5})$$

The longitudinal and transversal susceptibilities can be computed in terms of the matrix elements $\chi_{\sigma_1\sigma_2\sigma_3\sigma_4}$ as

$$\chi_{\text{long}}(\mathbf{q}, i\omega_l) = \chi_{\uparrow\uparrow\uparrow\uparrow}(\mathbf{q}, i\omega_l) - \chi_{\uparrow\downarrow\downarrow\uparrow}(\mathbf{q}, i\omega_l) \quad (\text{S6})$$

and

$$\chi_{\text{trans}}(\mathbf{q}, i\omega_l) = \chi_{\uparrow\uparrow\downarrow\downarrow}(\mathbf{q}, i\omega_l), \quad (\text{S7})$$

respectively. Note that the elements (1, 4) and (4, 1) of \hat{U} enter in the bubble summation, while the elements (2, 3) and (3, 2) enter in the ladder summation in Fig. S1.

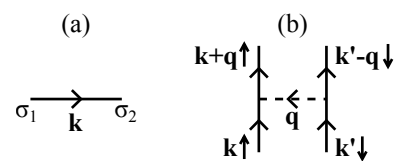


FIG. S2: (a) Diagram of the 2×2 fermionic propagator, Eq. (S2). (b) Diagram of the four leg interaction vertex U , corresponding to the second term in Eq. (1) of the main text.

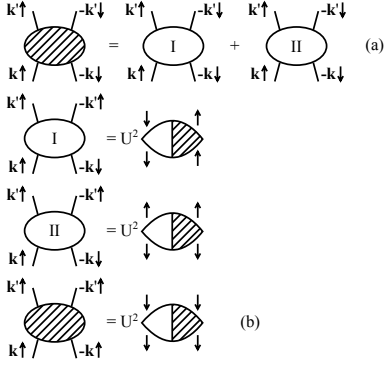


FIG. S3: These diagrams depict the effective interactions for (a) opposite spin projections and (b) same spin projections.

II. DERIVATION OF THE EFFECTIVE PARING INTERACTIONS

The effective spin-fluctuation-mediated interaction can be computed within the random phase approximation (RPA)[25, 26]. It can be decomposed into same spin projections $V_{\text{same}}^{\text{eff}}(\mathbf{k}, \mathbf{k}')$ and opposite spin projections $V_{\text{opp}}^{\text{eff}}(\mathbf{k}, \mathbf{k}')$. The effective interaction for opposite spin has two contributions, as shown in Fig. S3(a), which can be written as

$$V_{\text{opp}}^{\text{eff}}(\mathbf{k}, \mathbf{k}') = U^2 \chi_{\sigma\bar{\sigma}\bar{\sigma}\sigma}(\mathbf{k} - \mathbf{k}') + U^2 \chi_{\sigma\sigma\bar{\sigma}\bar{\sigma}}(\mathbf{k} + \mathbf{k}'). \quad (\text{S8})$$

The effective interaction for same spin projections, on the other hand, has only one contribution [see Fig. S3(b)] and is expressed as

$$V_{\text{same}}^{\text{eff}}(\mathbf{k}, \mathbf{k}') = U^2 \chi_{\sigma\sigma\sigma\sigma}(\mathbf{k} - \mathbf{k}'). \quad (\text{S9})$$

Using these effective interactions and employing a standard BCS approach, focusing on temperatures T close to T_c , we obtain the following linearized gap equations for the singlet (s) and triplet (t) channels in weak coupling

$$\Delta_{\alpha}^{\text{s/t}}(k) = \ln \left(\frac{1.13 \omega_c}{T_c} \right) \sum_{\beta} \int_{\text{FS}_{\beta}} \frac{dk'}{v_F^{\beta}(k')} V_{\text{s/t}}^{\text{eff}}(k, k') \Delta_{\beta}^{\text{s/t}}(k'), \quad (\text{S10})$$

where $\alpha, \beta = 1, 2$ label the FS sheets. Here, k and k' are restricted to the Fermi sheets FS_{α} and FS_{β} , respectively, $v_F^{\alpha}(\mathbf{k}) = |\nabla_{\mathbf{k}} E_{\mathbf{k}}^{\alpha}|$ is the Fermi velocity, and ω_c denotes the cutoff frequency, which is given by the energy scale of the magnetic fluctuations. In the case of singlet pairing the effective interaction $V_{\text{s}}^{\text{eff}}$ in Eq. (S10) originates only from scattering between electrons with opposite spins, i.e., we set $V_{\text{s}}^{\text{eff}}(k, k') = V_{\text{opp}}^{\text{eff}}(k, k')$. For triplet pairing, both equal- and opposite-spin scattering processes can yield a solution to Eq. (S10). We therefore solve Eq. (S10) for both $V_{\text{t}}^{\text{eff}}(k, k') = V_{\text{same}}^{\text{eff}}(k, k')$ and $V_{\text{t}}^{\text{eff}}(k, k') = V_{\text{opp}}^{\text{eff}}(k, k')$.

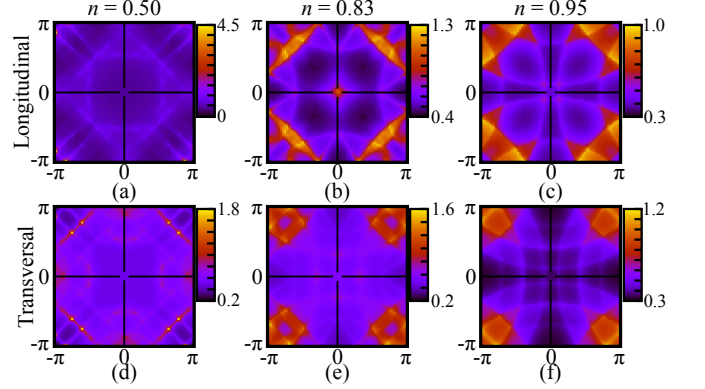


FIG. S4: Longitudinal and transverse RPA spin susceptibilities for the fillings $n = 0.50$, $n = 0.83$, and $n = 0.95$, respectively, with $t' = 0.3$, $V_{\text{so}} = 0.5$, $k_B T = 0.01$, and $U = 2.2$. The corresponding plots for $U = 0.4$ are shown in Fig. 1 of the main text.

In order to determine the symmetries of the pairing instabilities, we decompose the superconducting order parameter into an amplitude and a dimensionless symmetry function $\eta_i(k)$ for each pairing channel i . That is, we write $\Delta_{\alpha}^{\text{s/t}}(k) = \Delta_{\alpha} \eta_i(k)$, where $\eta_i(k)$ describes the k dependence of each possible pairing symmetry on the square lattice:

$$\eta_s = 1, \quad \eta_{d_{x^2-y^2}} = \cos k_x - \cos k_y, \quad \eta_{d_{xy}} = \sin k_x \sin k_y, \\ \eta_p = \sin k_x, \quad \eta_f = (\cos k_x - \cos k_y) \sin k_x. \quad (\text{S11})$$

Inserting the decomposition $\Delta_{\alpha}^{\text{s/t}}(k) = \Delta_{\alpha} \eta_i(k)$ into Eq. (S10), multiplying both sides of the equation by $\eta_i(k)$, and integrating over k yields

$$\Delta_{\alpha} = \ln \left(\frac{1.13 \omega_c}{T_c} \right) \sum_{\beta} \lambda_i^{\alpha\beta} \Delta_{\beta}, \quad (\text{S12})$$

for each pairing channel i . Here, $\lambda_i^{\alpha\beta}$ defines a 2×2 dimensionless pairing strength, which is given by [32–34]

$$\lambda_i^{\alpha\beta} = - \frac{\int_{\text{FS}_{\alpha}} \frac{dk}{v_F^{\alpha}(k)} \int_{\text{FS}_{\beta}} \frac{dk'}{v_F^{\beta}(k')} \eta_i(k) V_{\text{s/t}}^{\text{eff}}(k, k') \eta_i(k')}{2\pi^2 \int_{\text{FS}_{\beta}} \frac{dk'}{v_F^{\beta}(k')} [\eta_i(k')]^2}. \quad (\text{S13})$$

The diagonal and off-diagonal elements of $\lambda_i^{\alpha\beta}$ represent intra and inter FS pairing strengths, respectively. The effective superconducting coupling constant λ_i^{eff} for a given pairing channel i is determined by the largest eigenvalue of the matrix $\lambda_i^{\alpha\beta}$ [32], and allows to estimate T_c in first approximation by $T_c = 1.13 \omega_c e^{-1/\lambda_i^{\text{eff}}}$.

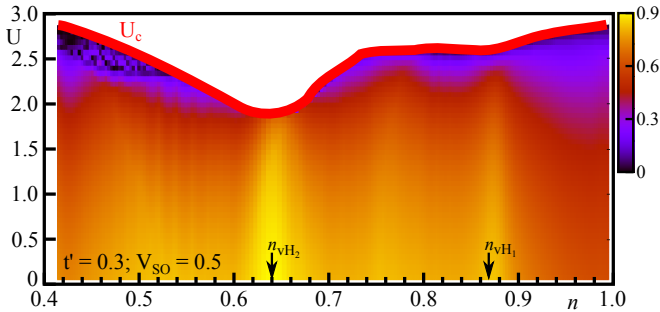


FIG. S5: Relative intensity of the ferromagnetic fluctuations in the transversal susceptibility as a function of interaction strength U and filling n . The red line indicates the critical interaction strength U_c . The corresponding plot for the longitudinal

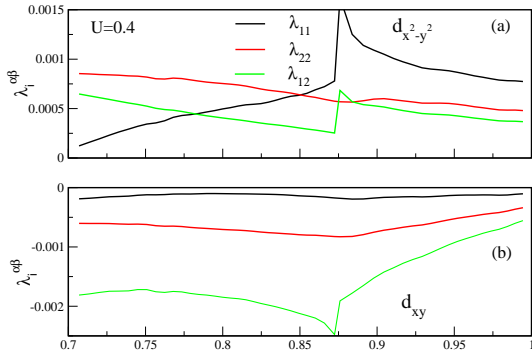


FIG. S6: Filling dependence of the intra and inter FS pairing strengths for (a) the $d_{x^2-y^2}$ -wave and (b) the d_{xy} -wave pairing symmetry. The corresponding plot for the f -wave channel is shown in Fig. 3(c) of the main text.

IV. ADDITIONAL PLOTS OF THE SPIN SUSCEPTIBILITY

In Fig. S4 we present plots of the longitudinal and transversal RPA spin susceptibility for three different fill-

ings and $U = 2.2$. Similar to Fig. 1 in the main text, we observe strong ferromagnetic fluctuations for $n = 0.83$ in the longitudinal susceptibility however, with lower intensity. Overall the \mathbf{q} space structure of the spin fluctuations is quite similar to Fig. 1 in the main text.

In Fig. S5 we show the relative strength of the ferromagnetic fluctuations in the transversal susceptibility as a function of U and filling n . In contrast to the longitudinal susceptibility shown in Fig. 2 in the main text, dominant ferromagnetic fluctuations only exist in very narrow regions around the two van Hove fillings n_{vH_1} and n_{vH_2} .

V. ADDITIONAL PLOTS OF THE PAIRING STRENGTH

In Figs. S6(a)-S6(b) we present the filling dependence of the intra FS (λ_i^{11} and λ_i^{22}) and the inter FS (λ_i^{12}) pairing strengths for the $d_{x^2-y^2}$ -wave and d_{xy} -wave pairing symmetry. We observe that the $d_{x^2-y^2}$ -wave instability is due to scattering within the Fermi sheet FS₁. The case of d_{xy} -wave channel is interesting: We find that both inter and intra FS pairing strengths are negative (repulsive), similar to the single FS case ($V_{SO} = 0$) where d_{xy} -wave superconductivity is absent [25]. However, in a two-band superconductor with two FSs, as for $V_{SO} \neq 0$, large negative inter FS interactions (green line) can drive pairing instabilities [32, 33]. In the present case this occurs for both the d_{xy} -wave channel [Fig. S6(b)] and the p -wave channel (not shown).